COMMUNICATIONS CHEMISTRY

ARTICLE

https://doi.org/10.1038/s42004-019-0191-7 OPEN

Proton-free electron-trapping feature of titanium dioxide nanoparticles without the characteristic blue color

Yan Yan[1,2], Weidong Shi[2], Wei Peng[1], Yuhan Lin[1], Chunxi Zhang[1,3], Lailai Li[4], Young Sun[3,4], Huanxin Ju[5], Junfa Zhu[5], Wanhong Ma[1,3] & Jincai Zhao[1,3]

Most solar-energy conversion applications are based on trapping and transferring photo-induced electrons on oxide semiconductor nanoparticles, such as titanium dioxide, and broad UV-vis absorption (400~800 nm) and monotonic IR absorption (1100~3000 cm^{-1}) signals have long been considered signatures of the electron-trapping state on titanium dioxide nanoparticles. Here we show that, under proton-free conditions and using iodide ions in acetonitrile as the hole scavenger, the intrinsic electron-trapping feature of titanium dioxide nanoparticles does not exhibit the characteristic UV-vis absorption and infrared absorption signatures. Further electron spin resonance studies identify the proton-free electron-trapping state as the lattice octahedral Ti_{6c}^{3+} species, differing from the traditional proton-participating surface tetrahedral Ti_{4c}^{3+} species. Synchronized radiation ultraviolet photoelectron spectroscopy results also show that the internal electron-trapping state without protons has a larger Ti_{3d} binding energy (1.8 eV) than the blue electron-trapping state (1.3 eV) that forms when protons participate and thus shows different electron transfer abilities.

[1] Beijing National Laboratory for Molecular Sciences, Key Laboratory of Photochemistry, CAS Research/Education Center for Excellence in Molecular Sciences, Institute of Chemistry, The Chinese Academy of Sciences, Beijing 100190, China. [2] School of Chemistry and Chemical Engineering, Jiangsu University, No. 301, Xuefu Road, Zhenjiang 212013, China. [3] University of Chinese Academy of Sciences, Beijing 100049, China. [4] State Key Laboratory of Magnetism and Beijing National Laboratory for Condensed Matter Physics, Institute of Physics, Chinese Academy of Sciences, Beijing 100080, China. [5] National Synchrotron Radiation Laboratory, University of Science and Technology of China, Hefei, Anhui 230029, China. Correspondence and requests for materials should be addressed to W.M. (email: whma@iccas.ac.cn) or to J.Z. (email: jczhao@iccas.ac.cn)

Metastable photoinduced electrons can be generated and constantly trapped on oxide semiconductor (e.g., TiO_2) nanoparticles in the presence of hole scavengers (e.g., H_2O, amines and alcohols)[1–3]. These trapped electrons can be used in situ or ex situ as very effective reducing reagents to accomplish many useful and challenging chemical reactions without extra high-temperature and high-pressure conditions, such as photocatalytic CO_2 reduction[4], water splitting for H_2 evolution[5], photochemical nitrogen fixation[6], and dehalogenation of halogenated organic compounds[7,8]. The site locations and states of trapped electrons (e^-_{cb}) on the conduction band of TiO_2 nanoparticles significantly influence the efficiency of the corresponding reactions[9,10]. Generally, photoinduced electrons in an anaerobic suspended system can be trapped at surface defect sites, such as the tetrahedral Ti_{4c}^{3+} species on TiO_2 nanoparticles[11,12], or in the bulk, such as the Ti_{6c}^{3+} species[12,13]. Alternatively, the electrons may also delocalize on the conduction band as free electrons[14]. The photoinduced electron selection of trapping locations on TiO_2 nanoparticles has been considered to mainly depend on the crystalline structure of TiO_2[12,14]. In addition, a recent picosecond XAS study demonstrated that the locations of trapped electrons on TiO_2 nanoparticles from dye sensitization and direct UV excitation are also different[15]. Although the final location of trapped electrons on TiO_2 nanoparticles is still controversial, TiO_2 nanoparticles with trapped electrons, no matter which hole scavenger is used, always exhibit broad visible-light absorption in the range of 400–800 nm[16–18] and broadband IR absorption from 1100 to 3000 cm^{-1} [19–22]. Such characteristic UV-vis and IR absorption with a distinct blue color has long been used to recognize and confirm surface Ti^{3+} species as the electron-trapping states on TiO_2 nanoparticles, as further evidenced by low-temperature (77 and 4 K) electron spin resonance (ESR) results[13], and is denoted as the blue state[22,23]. These blue-state trapped electrons have been quantitatively titrated by Fe^{3+}-1,10-phenanthroline reagent or TEMPO·/$_t$Bu$_3$ArO· radicals[16,19]. However, these insights on the blue state on TiO_2 nanoparticles were obtained under conditions using protic aqueous/alcohol solvents or with organic compounds as hole scavengers, and protons were available to mediate or stabilize electron trapping. We argue that the UV-vis and IR absorption characteristic of the electron-trapping features is only associated with proton participation. Until now, few other electron-trapping states have been discovered and reported on TiO_2 nanoparticles that do not exhibit the above signature.

Here we report the photoinduced electron-trapping feature of TiO_2 nanoparticles with iodide ions as a hole scavenger under strictly proton-free conditions. This feature is completely different from the common blue state observed under proton-participating conditions and does not exhibit the characteristic UV-vis (400–800 nm) and IR absorption (1100–3000 cm^{-1}). The ESR (4 K) studies indicated that these proton-free trapped electrons (I^- hole scavenger) almost all entered the bulk of the TiO_2 nanoparticles as the interstitial six-coordinated Ti_{6c}^{3+} species, which is distinct from the common proton-participating electron-trapping state (alcohol hole scavenger) of the surface four-coordinated Ti_{4c}^{3+} species. The synchrotron radiation ultraviolet photoelectron spectroscopy (SR-UPS) studies showed that the Ti_{3d} binding energy of the proton-free trapped electrons (1.8 eV) is higher than that of the blue-state trapped electrons with protons (1.3 eV), together with Fe(III)-1,10-phenanthroline titration and ESR $\cdot O_2^-$ detection, suggesting the different electron transfer abilities of the two electron-trapping states. Our work reveals that the well-known blue state exclusively occurs with the participation of available protons. To the best of our knowledge, this is the first reported scenery of trapped electrons on TiO_2 nanoparticles without both characteristic UV-vis and IR absorption as diagnostic signatures.

Results

Spectroscopic characteristics of trapped electrons. We designed two anaerobic liquid/TiO_2 (anatase, 15-nm-sized nanocrystals) suspended systems, one proton and one proton-free, to observe the photoinduced electron-trapping states. In the proton system, methanol was employed as both the protic solvent and hole scavenger. In the proton-free system, I^- ions (LiI) dissolved in acetonitrile (MeCN, an aprotic solvent) were employed as the hole scavenger. Under UV illumination and anaerobic conditions, photoinduced holes (h_{vb}^+) were eliminated by either methanol or I^- ions, and the corresponding photoinduced electrons were subsequently kept on the TiO_2 nanoparticles. When methanol was used, the illuminated TiO_2 nanoparticles always exhibited a broad UV-vis absorption peak at 725 nm (determined by the in situ optical-fiber UV-vis spectroscopy) (Fig. 1a) and a blue color (inset of Fig. 1a), which has been universally observed and denoted as the signature of the electron-trapping state on TiO_2 nanoparticles[16,18,19]. However, with LiI/MeCN, we unexpectedly did not observe the characteristic UV-vis absorption signal at ~700 nm. Instead, we only observed low absorption from 400 to 600 nm (Fig. 1b), which is from the I_3^- formed by the oxidation of I^- by photoinduced holes (refer to the standard UV-vis absorption spectra of I_3^- below in the inset of Fig. 1b and Supplementary Fig. 1). Rather than the traditional blue color, the illuminated TiO_2 nanoparticle suspension in LiI/MeCN exhibited a faint yellow color (top inset of Fig. 1b). By separating pre-illuminated TiO_2 nanoparticles from methanol and LiI/MeCN solutions, we further characterized the UV-vis diffused reflection spectra (UV-vis DRS) of different samples (Supplementary Fig. 2). Result shows that the signature absorption of electron-trapping state around 700 nm can only be observed on the pre-illuminated TiO_2 nanoparticles from methanol solution, which is consistent with the optical-fiber UV-vis absorption spectra.

We further quantitatively measured the saturated amount of trapped electrons on TiO_2 nanoparticles under the two conditions. With methanol, the trapped electrons from the oxidation of methanol ($CH_3OH + 2h_{vb}^+ \rightarrow CH_2=O + 2H^+$) were quantified by titration with the Fe(III)-1,10-phenanthroline titrant ($Fe^{3+} + e_{cb}^- +$ 1,10-phenanthroline $\rightarrow Fe^{2+}$-1,10-phenanthroline) (Fig. 1c). For the 0.6 g/L TiO_2 nanoparticles in the suspension, the saturated concentration of the trapped electrons was 1.7×10^{-4} M, accounting for 2.83×10^{-4} mol·g^{-1} on the TiO_2 nanoparticles, which is similar to the value determined in our previous work[19]. With LiI/MeCN, the common UV-vis absorption signature at ~725 nm and the blue color were lacking, but the trapping of photoinduced electrons was also confirmed and quantified by the spectroscopic determination of I_3^- formation (Supplementary Fig. 3). The saturated concentration of trapped electrons in the suspension was calculated as 0.7×10^{-4} M for the same TiO_2 concentration (0.6 g/L), which corresponds to 1.17×10^{-4} mol·g^{-1} on the TiO_2 nanoparticles. The saturated concentration of trapped electrons with LiI/MeCN is less than that with methanol. Mayer's group once observed a similar phenomenon on ZnO nanoparticles; i.e., more electrons were trapped (with $CoCp^*_2$, Cp^*= pentamethylcyclopentadienyl) under acidic conditions than basic conditions, and proposed that protons may facilitate the trapping of electrons on MO_x semiconductors[24].

We also verified whether the trapped electrons on the TiO_2 nanoparticles with LiI/MeCN can react with the Fe(III)-1,10-phenanthroline reagent. To avoid the presence of I^-, we separated the illuminated TiO_2 nanoparticles from the LiI/MeCN solution and then thoroughly washed the TiO_2 nanoparticles with

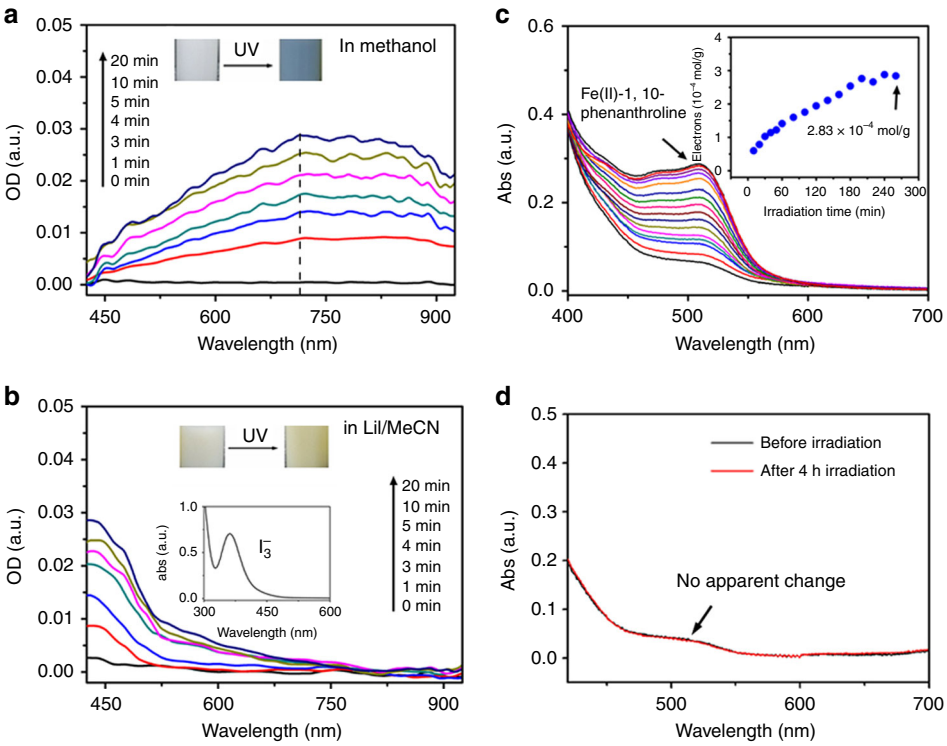

Fig. 1 Optical-fiber UV-vis absorption spectra. **a** In situ optical-fiber UV-vis absorption spectra of TiO_2 nanoparticles suspended in methanol under constant 365 nm illumination. The dashed line shows the peak at 725 nm. The inset shows the color change in the TiO_2 suspension before and after UV illumination. **b** Same conditions as (**a**) except the TiO_2 nanoparticles were suspended in a 0.1 M LiI/MeCN solution. The inset shows the color change of the TiO_2 suspension before and after illumination, and the standard UV-vis absorption spectra of the I_3^-/MeCN solution. **c** Spectroscopic titration of trapped electrons on TiO_2 nanoparticles (0.6 g/L) in methanol with different illumination times using the Fe(III)-1,10-phenanthroline titrant. The inset shows the corresponding electron concentration as a function of the illumination time (calculated from the absorption of Fe(II)-1,10-phenanthroline at 515 nm). The arrow indicates the saturated electron concentration. **d** The identical titrations of thoroughly washed TiO_2 nanoparticles (0.6 g/L) before and after 4 h UV illumination in a 0.1 M LiI/MeCN solution. No obvious change was found

MeCN. However, after the addition of the Fe(III)-1,10-phenanthroline titrant, no red Fe(II)-1,10-phenanthroline compound was generated (Fig. 1d), but the photoinduced electrons (1.17×10^{-4} mol·g^{-1}) were present on the TiO_2 nanoparticles, as evidenced by the I_3^- formation (Supplementary Fig. 3). This result demonstrates that the photoinduced electron-trapping states under proton and proton-free conditions have different electron transfer abilities for Fe(III)-1, 10-phenanthroline reduction. We further used ESR spectra to detect $\cdot O_2^-$ radicals as the product of the reaction between O_2 and TiO_2 nanoparticles in different systems under UV illumination ($O_2 + e_{cb}^- \rightarrow \cdot O_2^-$). We found that the $\cdot O_2^-$ signals can only be observed when TiO_2 nanoparticles suspended in methanol (Supplementary Fig. 4a). With the TiO_2/LiI/MeCN system, we only observed a background signal that is similar to the signal in the neat LiI/MeCN solution without TiO_2 nanoparticles (Supplementary Fig. 4b, c). This result indicates that photoinduced electrons under the proton-free condition are also not able to react with O_2 to produce $\cdot O_2^-$ radicals, which agrees with our Fe(III)-1,10-phenanthroline titration experiments.

ATR-FTIR spectroscopy is another typical method used for in situ observation of the electron-trapping state on TiO_2 nanoparticles. With methanol, we observed a very broad IR absorption band (3000–1100 cm^{-1}) that gradually increased with the UV irradiation time, as expected (Fig. 2a), and this band has always been ascribed to photoinduced electron-trapping state of Ti^{3+} species on TiO_2 nanoparticles[19–22]. However, such a diagnostic IR absorption band was not observed in the proton-free LiI/MeCN system (Fig. 2b), even with a prolonged reaction time (extended to 60 min). Moreover, when we added 10% H_2O as a proton donor to the same LiI/MeCN system, the diagnostic IR absorption band of the Ti^{3+} electron-trapping state appeared along with negative peaks at 1640 and 3300 cm^{-1} that were identified as the loss of H_2O by dissociation or oxidation (Fig. 2c)[25,26]. In this system, we also observed the UV-vis absorption peak at 725 nm, i.e., the signature of the blue-state trapped electrons, for the TiO_2 nanoparticles (Supplementary Fig. 5). To further exclude the oxidation of H_2O and only evaluate the effect of the proton donor in the proton-free LiI/MeCN system, we preloaded another inorganic proton donor, H_3PO_4, onto the TiO_2 surface and dried the sample to remove residual H_2O. As expected, under UV illumination, the broad IR absorption band at 3000–1100 cm^{-1} emerged but without the negative peaks at 1640 and 3300 cm^{-1} from the loss of H_2O (Fig. 2d). This result clearly demonstrates that when proton donors are present in a system, even with I^- as the electron donor, the electron-trapping feature in the LiI/TiO_2/MeCN system will change to the proton model as observed with methanol. By designing the proton-free LiI/MeCN system, we successfully revealed that the characteristic UV-vis and IR absorption signatures of the blue-state trapped electrons only occur in the presence of available protons. However, why do the proton-free trapped electrons on TiO_2 nanoparticles not exhibit the characteristic UV-vis and IR absorption signals? What is the significant difference between the proton-free electron-trapping state and the common proton blue state?

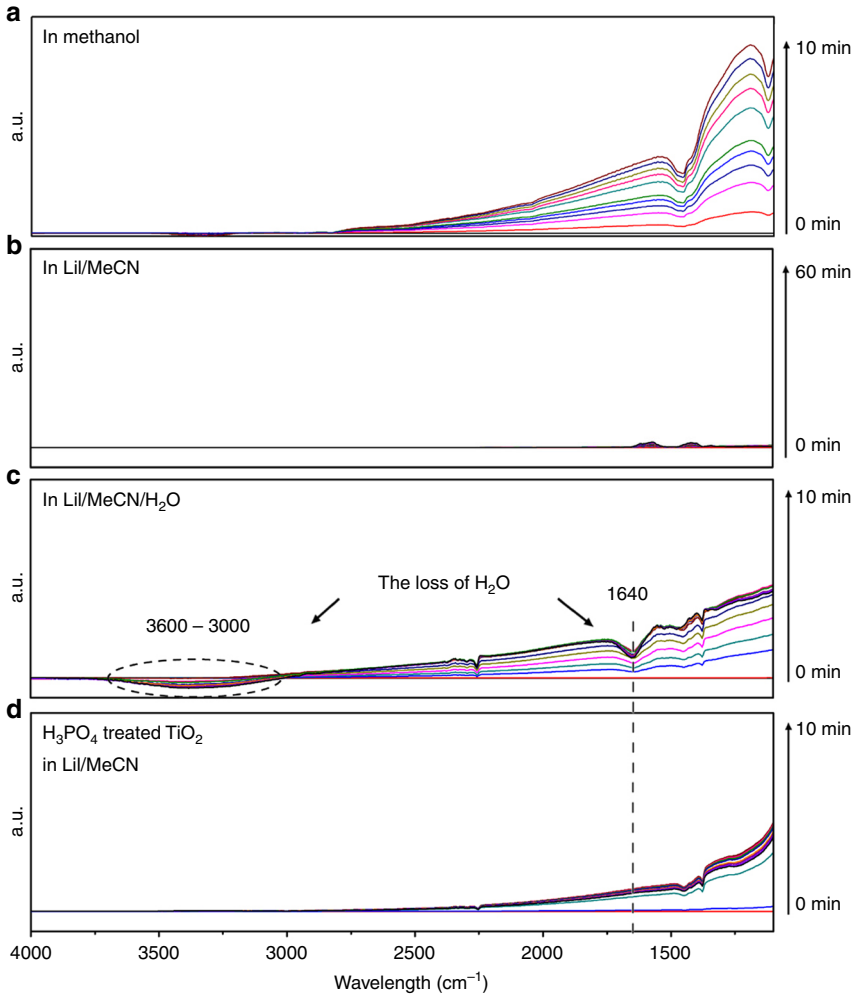

Fig. 2 In situ ATR-FTIR spectra on difference systems. **a** TiO_2 film immersed in methanol; **b** TiO_2 film immersed in a 0.1 M LiI/MeCN solution; **c** TiO_2 film immersed in a 0.1 M LiI/MeCN/H_2O (vMeCN:vH_2O = 9:1) solution. The dashed circle and lines show the signal of water. **d** H_3PO_4-pretreated TiO_2 film immersed in a 0.1 M LiI/MeCN solution. All experiments were conducted in an Ar atmosphere

ESR and SR-UPS characterizations. We used low-temperature (4 K) ESR and synchrotron radiation ultraviolet photoelectron spectroscopy (SR-UPS) to characterize the different photoinduced electron-trapping states on TiO_2 nanoparticles. Trapped electrons in the form of Ti^{3+} can be easily recognized by their distinct ESR signals[12,13,27,28]. In 1985, Howe and Grätzel first observed in detail the electron-trapping locations in anaerobic, colloidal TiO_2 aqueous suspensions by low-temperature (77 and 4 K) ESR[13]. They distinguished the surface Ti^{3+} species from the interstitial Ti^{3+} species in the bulk TiO_2 nanoparticles and suggested that increasing the acidity and temperature of the TiO_2 nanoparticle suspension favors the trapping of photoinduced electrons in surface sites[13]. However, since their observations were all carried out in aqueous solutions (H_2O can be considered a common proton and electron donor under most conditions), their conclusion was that different hole scavengers (i.e., proton-containing and proton-free scavengers), such as methanol, I^- and polyvinyl alcohol (PVA), do not have a substantial influence on the Ti^{3+} species formed, but this conclusion is valid only in reaction systems with available protons. Under our experimental conditions, i.e., with methanol (Fig. 3a), we observed a rapidly increasing signal peak at $g = 1.979$ in the ESR spectrum with increasing UV illumination time. For illumination times over 4 h, a weak ESR signal at $g_{\|} = 1.930$ was observed. The strong signal at $g = 1.979$ is attributed to surface distorted four-coordinate tetrahedral $Ti_{4c}{}^{3+}$ species, while the weak signal peak at $g_{\|} = 1.930$ is attributed to anatase surface six-coordinate octahedral $Ti_{6c}{}^{3+}$ species[12,13,27,28]. We obtained the same ESR signals using ethanol and isopropanol instead of methanol as the proton-containing electron donors (Supplementary Fig. 6a, b). This result agrees with many other previous observations on the use of different organic compounds or H_2O as proton and electron donors[12,13,27,28], indicating that photoinduced electrons are trapped mainly as surface $Ti_{4c}{}^{3+}$ species with some surface $Ti_{6c}{}^{3+}$ species on TiO_2 nanoparticles in the presence of protons. However, with LiI/MeCN (Fig. 3b), we did not observe the signals for surface $Ti_{4c}{}^{3+}$ and $Ti_{6c}{}^{3+}$ species at $g = 1.979$ and $g_{\|} = 1.930$, respectively, with increasing UV illumination time. Instead, we only observed an increasing peak at $g_{\perp} = 1.990$ that corresponds to the anatase lattice octahedral $Ti_{6c}{}^{3+}$ state[12,13], which never appeared with methanol. When using NaI instead of LiI as the proton-free electron donor, we also observed the signal of the interstitial lattice $Ti_{6c}{}^{3+}$ state (Supplementary Fig. 6c). This result indicates that photoinduced electrons are trapped as interior interstitial $Ti_{6c}{}^{3+}$ species in the lattice of the TiO_2 nanoparticles in the I^-/MeCN system without the participation of protons. Without I^- in MeCN, the signal of Ti^{3+} species can no longer be observed (Supplementary Fig. 7). In addition, we added 10% H_2O (pH = 1–13, adjusted by $HClO_4$ and NaOH) as a controllable proton donor into identical LiI/MeCN suspension systems to

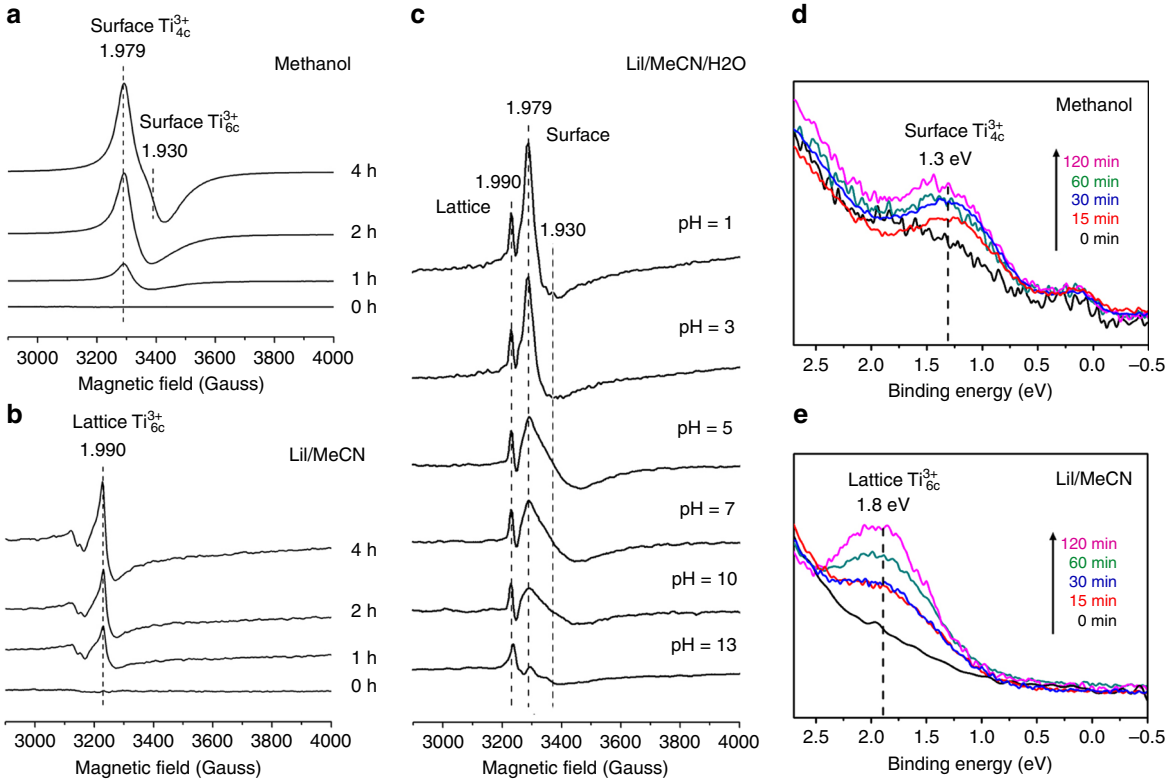

Fig. 3 ESR collected at 4 K and SR-UPS characterizations. **a** ESR spectra of TiO_2 nanoparticles in methanol with different UV illumination (365 nm, 100 W) times (1–4 h). **b** Same conditions as (**a**) except TiO_2 nanoparticles were suspended in a 0.1 M LiI/MeCN solution. **c** ESR spectra of TiO_2 nanoparticles in a 0.1 M LiI/MeCN/H_2O solution (vMeCN:vH_2O = 9:1) after 4 h of UV illumination with the pH of the water adjusted from 13 to 1. **d** SR-UPS spectra (Ti_{3d} orbital) of TiO_2 nanoparticle films after UV illumination for different times (0–120 min) in methanol. **e** Conditions identical to those in (**d**) except the TiO_2 nanoparticle films were illuminated in a 0.1 M LiI/MeCN solution

observe if the electron-trapping states changed from lattice Ti_{6c}^{3+} species to surface Ti_{4c}^{3+} species. Indeed, with the addition of H_2O, we observed that the signal of the surface Ti_{4c}^{3+} species at $g = 1.979$ reappeared in the LiI/MeCN/H_2O system, and its intensity gradually increased as the pH value of H_2O decreased relative to the lattice Ti_{6c}^{3+} signal at $g_\perp = 1.990$ (Fig. 3c). Notably, a separate ESR signal for the interior interstitial Ti_{6c}^{3+} species on TiO_2 nanoparticles was also obtained by Howe and Grätzel in a frozen aqueous solution when they illuminated a TiO_2 sample at 77 K without hole scavengers[13]. In contrast to the sample illuminated at room temperature, in which the surface Ti^{3+} state dominates, illumination of their frozen system at ultralow temperature resulted in interior trapping of photoinduced electrons on TiO_2 nanoparticles even in the presence of H_2O[13]. Their observation is not contradictory to ours; i.e., the presence of available protons causes photoinduced electrons to be trapped on the surface of TiO_2 nanoparticles as Ti_{4c}^{3+} species, since proton formation and transfer are significantly inhibited at ultralow temperatures in a frozen system. Correspondingly, in our strictly proton-free I^-/MeCN system, we obtained the separate interior Ti_{6c}^{3+} species on TiO_2 nanoparticles by merely illuminating the TiO_2 sample at room temperature. Thus, our work indicates that the occurrence and disappearance of the typical UV-vis and IR adsorption signatures for the electron-trapping event are essentially dependent on the location of the trapped electrons on the surface or interior lattice of the TiO_2 nanoparticles, which is controlled by the presence or absence of protons. The conventional blue state on TiO_2 nanoparticles requires available protons to stabilize trapped electrons as surface Ti_{4c}^{3+} species.

We further measured the Ti_{3d} binding energy of the different electron-trapping states on TiO_2 nanoparticles by SR-UPS (near the Fermi edge, 0–3 eV). Anatase TiO_2 nanocrystal films were coated on a piece of Ti foil (see Methods section) and illuminated by UV light (365 nm) in methanol and LiI/MeCN solutions. The illuminated TiO_2 films were subsequently washed with MeCN, dried, and transferred under anaerobic conditions for the SR-UPS characterizations. With methanol, the Ti_{3d} binding energy of the photoinduced electron-trapping state on the TiO_2 nanoparticle film was observed at 1.3 eV (Fig. 3d), which is larger than that of the well-known Ti_{3d} defect state at 0.85 eV due to the construction of bridging oxygen vacancies (see Supplementary Fig. 8)[29]. However, with LiI/MeCN, the Ti_{3d} binding energy of the electron-trapping state significantly shifted to 1.8 eV (Fig. 3e). This 0.5 eV difference in the binding energy of the Ti_{3d} orbital directly reveals that the electrons trapped on TiO_2 nanoparticles in the presence of methanol are much easier to lose than those trapped in the LiI/MeCN system, which explains why the trapped electrons in the LiI/MeCN system cannot react with the Fe(III)-1,10-phenanthroline titrant and O_2.

Discussion

In summary, we experimentally revealed the electron-trapping feature of TiO_2 nanoparticles without the participation of protons, which does not exhibit the well-known UV-vis (400–800 nm) and IR absorption signals (1100–3000 cm^{-1}). In the well-known blue state stabilized by protons, photoinduced electrons tend to be trapped as surface tetrahedral Ti_{4c}^{3+} species on TiO_2 nanoparticles. However, the electron-trapping state without available protons tends to be interior interstitial octahedral Ti_{6c}^{3+} species in the lattice of the TiO_2 nanoparticles. Fe(III)-1,10-phenanthroline titration experiments, ESR·O_2^- detection and SR-

UPS spectra showed the different electron transfer abilities of the two kinds of electron-trapping states. Our results shed light on the intrinsic electron-trapping behaviors of TiO_2 nanoparticles that were previously hidden under numerous proton-participating conditions. This basic insight into electron trapping in oxide semiconductors provides more information for the future design and preparation of efficient TiO_2-based solar energy conversion devices.

Methods

Chemicals. The typical titanium dioxide (TiO_2) solid sample, anatase TiO_2 (15 nm nanocrystals), was purchased from Alfa Aesar (Shanghai, China). If not specifically mentioned, the TiO_2 samples in all experiments were identical anatase TiO_2 nanoparticles. Anhydrous $FeCl_2$, $Fe(NO_3)_3$•$9H_2O$, 1,10-phenanthroline, acetic acid (HAc), perchloric acid ($HClO_4$, 70%), LiI (99.9%), methanol, and acetonitrile (MeCN) were purchased from Acros (Beijing, China) and used as received.

Instruments. UV-vis absorption spectra of Fe(II)-1,10-phenanthroline and I_3^- ions were recorded on a Hitachi U3900 (Japan) spectrometer. The in situ optical-fiber UV-vis absorption spectroscopy measurement system was based on the Ocean Optics (Shanghai, China) HL-2000-FHSA optical-fiber analysis machine. The in situ ATR-FTIR spectra were collected using a Nicolet 8700 FT-IR instrument equipped with a DTGS detector. Low-temperature ESR spectroscopy was recorded on a JEOL (Japan) JES-FA200 ESR spectrometer. The SR-UPS experiments were performed at the Catalysis and Surface Science Endstation (BL11U beamline) in the National Synchrotron Radiation Laboratory (NSRL), Hefei, China.

Photo-illumination of TiO_2 nanoparticle suspensions. In a typical procedure, a TiO_2 suspension (0.2–1.0 g/L) in methanol or 0.1 M LiI/MeCN was sealed into a 50-mL quartz bottle and degassed by argon for 30 min. Then, the quartz bottle was placed into a black box for UV illumination for different times (1–12 h). A high-power (100 W) 365-nm monochromatic LED lamp was employed as the UV light source.

In situ optical-fiber UV-vis absorption spectroscopy. We designed an in situ analysis system to measure the UV-vis absorption of TiO_2 suspensions (2.0 g/L). TiO_2 suspensions were held in a sealed quartz cube in a black box under constant UV (365 nm, 100 W) irradiation. UV-vis absorption spectra were recorded in situ from 400 to 900 nm by an optical-fiber spectrometer.

In situ ATR-FTIR analysis. The ATR-FTIR spectroscopy experimental setup consisted of Harrick Horizon multiple internal reflection accessories coupled to a 4 mL flow-through cell containing a ZnSe crystal on the bottom plate and a quartz window on the top plate. Eleven infrared bounces were allowed using a 45° internal reflection element ($50 \times 10 \times 2\ mm^3$). In a typical procedure, a layer of reaction solution (methanol or I^-/MeCN) was dripped onto the surface of a ZnSe crystal coated with a TiO_2 film. The apparatus was degassed with argon for 30 min, and the crystal was scanned to obtain the background spectrum. Time-resolved in situ FTIR data were collected under irradiation by a 365 nm LED lamp (3 W).

ESR analysis. Low-temperature (4 K) ESR spectra were collected using liquid helium as the coolant. In a typical procedure, photoreduced TiO_2 was sealed in a quartz tube in an argon atmosphere. The settings for the ESR spectrometer were as follows: center field = 3500 G, sweep width = 1000 G, microwave frequency = 9.52 GHz, and field modulation frequency = 100 kHz.

SR-UPS experiments. The near-Fermi level Ti_{3d} spectra (0–3 eV) were measured using synchrotron radiation light as the excitation source with a photon energy of 47.5 eV. In a typical procedure, anatase TiO_2 films were preilluminated in different reaction systems, washed with MeCN, dried in an argon glove box, and transferred into the SR-UPS ultrahigh vacuum system under the protection of an argon flow.

Fe(III)-1,10-phenanthroline spectrometric titration. Trapped electrons on UV-illuminated TiO_2 nanoparticles were quantitatively measured by the Fe(III)-1,10-phenanthroline titration spectrometric method. The 1,10-phenanthroline spectrometric titration is a simple, widely used method for the measurement of Fe(II) ions. Here, we used the Fe(III) solution to titrate the trapped electrons on TiO_2 nanoparticles and quantitatively produce Fe(II) ions. Then, we used 1,10-phenanthroline to measure the concentration of Fe(II) ions produced, thereby quantifying the concentration of trapped electrons. In a typical procedure, 2.5 mL of the UV-illuminated TiO_2 suspension was transferred to an argon glove box and mixed with 2.5 mL of a $Fe(NO_3)_3$ (10^{-3} M) solution. The resulting mixture was centrifuged. Then, 1.5 mL of the centrifuged supernatant was taken from the argon glove box and mixed with 1.5 mL of pH = 4.6 HAc-NaAc buffer solution. Then, 1 mL of a 0.2% 1,10-phenanthroline aqueous solution was added to obtain a clear red solution. The resulting solution was transferred to a quartz cuvette and measured on a Hitachi U3900 spectrometer. For the sample in the I^-/MeCN system, the wash treatment of the TiO_2 nanoparticles was conducted in an argon glove box by MeCN, and then, the clean TiO_2 nanoparticles were suspended in MeCN for the titration measurement.

ESR O_2^- detection. ESR detection of $\cdot O_2^-$ radicals was conducted at room temperature on the Bruker E500 machine with DMPO as radical trapping reagent. In a typical procedure, 0.5 μg DMPO was added into 10 mL different liquid/TiO_2 suspended systems (with 0.6 g/LTiO_2). The resulting suspension was then collected by a capillary quartz tube for the ESR detection. During the detection, 355 nm pulse laser (1 kHz) was employed to constantly illuminate the sample. All experiments were conducted under the ambient condition.

Preparation of H_3PO_4-treated TiO_2 nanoparticles. In a typical procedure, 100 mg TiO_2 powder was dissolved in 5 mL of a diluted (5%) H_3PO_4 aqueous solution. Then, the suspension was dried at 70 °C overnight, and the resulting solid was ground into a powder to obtain H_3PO_4-treated TiO_2 for the ATR-FTIR measurement.

Preparation of TiO_2 nanoparticle films. TiO_2 films for SR-UPS experiments were loaded on 0.25-mm-thick Ti metal foil. In a typical procedure, TiO_2 was dissolved into n-butyl alcohol with the addition of several drops of polyethylene glycol tert-octylphenyl ether (Triton X-100) as a thickener. The solid solution ratio of the TiO_2 suspension was between 10 and 15%. After ultrasonic (for 1 h) and stirring treatments (for at least 1 day), the resulting suspension was used as the precursor for the TiO_2 films. The resulting precursor was coated on Ti metal foil by the traditional doctor-blade method and then calcined at 450 °C for 1 h to obtain the final product.

Data availability

The data that support the findings of this study are available from the corresponding author upon reasonable request.

Received: 26 February 2019 Accepted: 28 June 2019
Published online: 30 July 2019

References

1. Knorr, F., Mercado, C. & McHale, J. Trap-state distributions and carrier transport in pure and mixed-phase TiO_2: influence of contacting solvent and interphasial electron transfer. *J. Phys. Chem. C* **112**, 12786–12794 (2008).
2. Bowker, M. & Bennett, R. The role of Ti^{3+} interstitials in TiO_2(110) reduction and oxidation. *J. Phys. Condens. Matter* **21**, 474224 (2009).
3. Zhao, D., Chen, C., Yu, C., Ma, W. & Zhao, J. Photoinduced electron storage in WO_3/TiO_2 nanohybrid material in the presence of oxygen and postirradiated reduction of heavy metal ions. *J. Phys. Chem. C* **113**, 13160–13165 (2009).
4. Yu, J., Low, J., Xiao, W., Zhou, P. & Jaroniec, M. Enhanced photocatalytic CO_2-reduction activity of anatase TiO_2 by coexposed {001} and {101} facets. *J. Am. Chem. Soc.* **136**, 8839–8842 (2014).
5. Khan, S. U., Al-Shahry, M. & Ingler, W. B. Efficient photochemical water splitting by a chemically modified n-TiO_2. *Science* **297**, 2243–2245 (2002).
6. Yang, F. et al. The improvement of spinach growth by nano-anatase TiO_2 treatment is related to nitrogen photoreduction. *Biol. Trace Elem. Res.* **119**, 77–88 (2007).
7. Chang, W. et al. Inverse kinetic solvent isotope effect in TiO_2 photocatalytic dehalogenation of non-adsorbable aromatic halides: a proton-induced pathway. *Angew. Chem. Int. Ed.* **127**, 2080–2084 (2015).
8. Lv, Y. et al. Rapid photocatalytic debromination on TiO_2 with *in-situ* formed copper co-catalyst: Enhanced adsorption and visible light activity. *Appl. CataL. B-Environ.* **194**, 150–156 (2016).
9. Swierk, J. R., McCool, N. S., Saunders, T. P., Barber, G. D. & Mallouk, T. E. Effects of electron trapping and protonation on the efficiency of water-splitting dye-sensitized solar cells. *J. Am. Chem. Soc.* **136**, 10974–10982 (2014).
10. McCool, N. S. et al. Proton-induced trap states, injection and recombination dynamics in water-splitting dye-sensitized photoelectrochemical cells. *ACS Appl. Mater. Inf.* 8, 16727–16735 (2016).
11. Deskins, N. A., Rousseau, R. & Dupuis, M. Distribution of Ti^{3+} surface sites in reduced TiO_2. *J. Phys. Chem. C* **115**, 7562–7572 (2011).
12. Li, G. et al. The important role of tetrahedral Ti^{4+} sites in the phase transformation and photocatalytic activity of TiO_2 nanocomposites. *J. Am. Chem. Soc.* **130**, 5402–5403 (2008).
13. Howe, R. F. & Grätzel, M. EPR observation of trapped electrons in colloidal titanium dioxide. *J. Phys. Chem.* **89**, 4495–4499 (1985).

14. Setvin, M. et al. Direct view at excess electrons in TiO_2 rutile and anatase. *Phys. Rev. Lett.* **113**, 086402 (2014).
15. Rittmann-Frank, M. H. et al. Mapping of the photoinduced electron traps in TiO_2 by picosecond X-ray absorption spectroscopy. *Angew. Chem. Int. Ed.* **53**, 5858–5862 (2014).
16. Schrauben, J. N. et al. Titanium and zinc oxide nanoparticles are proton-coupled electron transfer agents. *Science* **336**, 1298–1301 (2012).
17. Halverson, A. F. et al. Perturbation of the electron transport mechanism by proton intercalation in nanoporous TiO_2 films. *Nano Lett.* **12**, 2112–2116 (2012).
18. Chen, C., Shi, T., Chang, W. & Zhao, J. Essential roles of proton transfer in photocatalytic redox reactions. *ChemCatChem* **7**, 724–731 (2015).
19. Yan, Y. et al. The formation of Ti–H species at interface is lethal to the efficiency of TiO_2-based dye-sensitized devices. *J. Am. Chem. Soc.* **139**, 2083–2089 (2017).
20. Warren, D. & McQuillan, A. Influence of adsorbed water on phonon and UV-Induced IR absorptions of TiO_2 photocatalytic particle films. *J. Phys. Chem. B* **108**, 19373–19379 (2004).
21. Szczepankiewicz, S., Moss, J. & Hoffmann, M. Slow surface charge trapping kinetics on irradiated TiO_2. *J. Phys. Chem. B* **106**, 2922–2927 (2002).
22. Panayotov, D. A. & Yates, J. T. n-Type doping of TiO_2 with atomic hydrogen-observation of the production of conduction band electrons by infrared spectroscopy. *Chem. Phys. Lett.* **436**, 204–208 (2007).
23. Peper, J. L., Vinyard, D. J., Brudvig, G. W. & Mayer, J. M. Slow equilibration between spectroscopically distinct trap states in reduced TiO_2 nanoparticles. *J. Am. Chem. Soc.* **139**, 2868–2871 (2017).
24. Valdez, C. N., Schimpf, A. M., Gamelin, D. R. & Mayer, J. M. Proton-controlled reduction of ZnO nanocrystals: effects of molecular reductants, cations, and thermodynamic limitations. *J. Am. Chem. Soc.* **138**, 1377–1385 (2016).
25. Zhang, H., Zhou, P., Ji, H., Chen, C. & Zhao, J. Enhancement of photocatalytic decarboxylation on TiO_2 by water-induced change in adsorption-mode. *Appl. CataL. B-Environ.* **224**, 376–382 (2018).
26. Zhang, H. et al. Hydrogen-bond bridged water oxidation on {001} surfaces of anatase TiO_2. *J. Phys. Chem. C* **121**, 2251–2257 (2017).
27. Hurum, D. C., Gray, K. A., Rajh, T. & Thurnauer, M. C. Recombination pathways in the degussa P25 formulation of TiO_2: surface versus lattice Mechanisms. *J. Phys. Chem. B* **109**, 977–980 (2005).
28. Hurum, D. C., Agrios, A. G., Gray, K. A., Rajh, T. & Thurnauer, M. C. Explaining the enhanced photocatalytic activity of degussa P25 mixed-phase TiO_2 using EPR. *J. Phys. Chem. B* **107**, 4545–4549 (2003).
29. Wendt, S. et al. The role of interstitial sites in the Ti_{3d} defect state in the band gap of titania. *Science* **320**, 1755–1759 (2008).

Acknowledgements

This work was supported by the NSFC (Nos. 21590811, 21521062, 21777167) and the "Key Research Program of Frontier Sciences" (NO. QYZDY-SSW-SLH028) of the Chinese Academy of Sciences.

Author contributions

Y.Y., W.M., and Ji.Z. conceived the idea, discussed, and analyzed the data. Y.Y. performed the majority of experiments and drafted the paper; W.P. and Y.L. performed the ESR $\cdot O_2^-$ detection experiments; L.L., Y.S., and C.Z. contributed the low-temperature ESR measurement; H.J. and Ju.Z. contributed the SR-UPS measurement; W.S. proposed valuable advice for improving the paper. All authors discussed the results and commented on the paper.

Additional information

Supplementary information accompanies this paper at https://doi.org/10.1038/s42004-019-0191-7.

Competing interests: The authors declare no competing interests.

Reprints and permission information is available online at http://npg.nature.com/reprintsandpermissions/

Publisher's note: Springer Nature remains neutral with regard to jurisdictional claims in published maps and institutional affiliations.